Effective Removal of Methylene Blue Dye Using Low-Cost Essential Oil Industry Waste: Novel Hybrid Design Approach, Kinetic and Thermodynamic Evaluation

Sourodipto Modak · Priyanka Katiyar ·
Geetesh Kumar · Sanjeev Yadav

Abstract This study utilizes spent carrot seed waste (SCSW) as an adsorbent for the removal of methylene blue dye from synthetic wastewater. The influence of reaction parameters—temperature, pH, time, dye concentration, adsorbent dose, and RPM—is studied to maximize the adsorption capacity and dye removal. The hybrid optimization design approach (DoE + manual) reveals that dye concentration and adsorbent dose are the primary influencing factors. SCSW exhibits a maximum adsorption capacity of 234 mg/g, achieving approximately 98% dye removal. Langmuir, Freundlich, and Temkin isotherms are employed, with the best fit observed at 50 °C. Kinetic analysis reveals that the adsorption process adheres to the pseudo-first and pseudo-second-order processes, as well as the Elovich model at all dye concentrations. The equilibrium models suggest that the adsorption of Methylene Blue dye molecules is monolayer and multilayer onto the heterogeneous surface of SCSW. The kinetic and thermodynamic studies imply that the adsorption process is exothermic and physico-chemical in nature.

Finally, regeneration of dye-coated SCSW is performed to check its reusability and found that thermochemical regeneration is the appropriate method for regeneration.

Keywords Carrot seed waste · Hybrid design approach · Adsorption isotherm · Kinetics · Waste management

1 Introduction

Essential oils are derived from diverse natural sources such as plants, flowers, seeds, leaves, roots, and stems, which have garnered significant attention due to their myriad health benefits. These oils find applications in aromatherapy, self-care products, food, and pharmaceuticals. The global market size for essential oils is projected to reach 18.96 billion dollars by 2023, with an annual growth rate of approximately 6%. This growth is particularly notable in Asian countries, including India and China (Abu Bakar et al., 2020). The expanding essential oil market is likely lead to an increase in the residues generated by essential oil industries. Presently, Europe alone generates approximately 700 million tonnes of industrial agricultural waste annually, and a significant portion of this waste remains underutilized (Truzzi et al., 2022). Spent carrot seed waste (SCSW) is another typical byproduct of the essential oil industry, commonly either discarded in landfills

S. Modak · P. Katiyar (✉) · G. Kumar · S. Yadav
Department of Chemical Engineering, Shiv Nadar Institution of Eminence (Deemed to be University), Greater Noida, Uttar Pradesh – 201314, India
e-mail: priyanka@snu.edu.in

or repurposed as cattle feed (Modak et al., 2023). The valorization of post-extraction solid wastes is crucial for effective waste management and contributes to the circular economy. Adsorption is considered a highly suitable method for utilizing such waste in terms of cost, design simplicity, operational ease, accessibility, and effectiveness, especially for treating industrial wastewater from various sectors such as textile, pulp and paper, pharmaceuticals, leather, and more (Gopal et al. 2014; Unugul and Nigiz 2020). It is reported that by 2050, the textile sector will quadruple water pollution, making it the second-largest polluting industry in the world (Kumar et al., 2021). Methylene blue (MB) is a popular cationic dye used by the textile industry causing adverse reactions like nausea, increased heart rate, diarrhea, vomiting, and gastrointestinal tract irritation (Ichipi et al., 2023). The environmental challenge of removing MB from industrial wastewater has become prominent (Oladoye et al., 2022). In this context, utilizing SCSW as an adsorbent serves two important purposes. Firstly, it provides an effective way to repurpose and make use of solid waste generated in the essential oil industry. Secondly, it addresses the need to clean industrial effluents, particularly those generated by industries such as textiles, pulp and paper, pharmaceuticals, and leather, which often contain pollutants like MB dye.

The adsorption process involves multiple operating parameters, having impact on dye removal efficiency, and determining the optimum parameters for effective pollutant removal requires a substantial number of experiments. The Design of Experiments (DoE) approach assists in identifying the appropriate experimental parameters that influence the adsorption process with the minimum number of experimental runs. Response Surface Methodology (RSM), a DoE approach, is employed to evaluate the significance of various influencing parameters while considering their interactions as well (Montgomery, 2017). The researchers have explored DoE approaches on various adsorbents such as sugarcane bagasse, peanut hull, orange peel, and mustard straw biochar and for the adsorption of MB dye (Jain et al., 2022), (Patidar & Vashishtha, 2020). Modak et al. (2023) conducted a comprehensive physico-chemical analysis of SCSW and established its suitability as an adsorbent for treating dye-containing wastewater. The inherent porous morphology and diverse surface functional groups and adsorption active

sites make it well-suited for this purpose. Nevertheless, there is a gap in the literature concerning a detailed investigation of MB dye adsorption onto SCSW as an adsorbent, particularly using an integrated approach that involves computational, modeling, and thermodynamic analyses.

Hence, this study employs two step optimization methodologies, namely screening design and hybrid CCD, for the first time to analyze the impacts of various adsorption parameters on adsorption capacity and dye removal efficiency of SCSW to treat MB dye wastewater. Subsequently, isotherm, kinetic, and thermodynamic studies are conducted to delve into the mechanisms underlying the adsorption of MB onto SCSW. Additionally, the regeneration and reutilization of dye-coated SCSW is explored to evaluate its shelf life as an adsorbent.

2 Material and Methods

2.1 Sample Procurement, Preparation, and Characterization

Methylene blue (MB) dye powder was procured from TCI Chemicals for making synthetic textile wastewater. The SCSW was procured from the Rajeshwari essential oil industry in Kannauj, India. It was washed repeatedly with DI water to remove the impurities and organic-laden compounds from the waste, then dried in an air oven at 70 °C for 12 h. Dried SCSW was stored in the zip bag for further utilization in the adsorption study. The physico-chemical characteristics of SCSW highlight its suitability as an adsorbent for removing cationic dyes from wastewater (Modak et al., 2023). FTIR and TPD analysis revealed the presence of oxygenated functional groups (C=O, OH, C–O) and strong acidic active sites, making SCSW highly favorable for cationic dye adsorption. FE-SEM analysis exhibited a heterogeneous porous morphology with honeycomb structures and ridges on the SCSW surface, providing an ideal surface for the adsorption of organic pollutants like cationic dyes.

2.2 Point of Zero Charge (pH_{pzc}) of SCSW Adsorbent

One of the crucial variables used to calculate the surface charge of the SCSW adsorbent is the point

of zero charge (pH$_{pzc}$). The pH drift method was used for the determination of pH$_{pzc}$ (Milonjić et al., 1975), where 50 ml of 0.01 M NaCl was introduced to 10 conical flasks with pH values ranging from 3 to 12, respectively. A pH adjustment was made using 0.1 M HCl and 0.1 M NaOH. After that, 0.15 g of SCSW sample was added to each conical flask, sealed, and incubated in an orbital shaking incubator for 48 h at 30 °C to achieve equilibrium. The filtrate from each conical flask was collected after 48 h, and pH$_{final}$ is determined using a pH meter. The ΔpH (pH$_{final}$ − pH$_{initial}$) vs pH$_{initial}$ plot was used to determine the pH$_{pzc}$ of SCSW adsorbent where ΔpH is zero. Three duplicates of each experiment were carried out.

2.3 Batch Adsorption Experiments

To perform adsorption experiments, 100 ml of MB dye solution of the desired concentration and pH was taken in a conical flask with the required amount of dried SCSW (particle size 0.6 mm) and kept in an orbital shaking incubator (Ambassador, India). The RPM, reaction time, and reaction temperature were set as per the experimental runs. Once the reaction time was over, the solution was filtered through 0.45-μm Wattman filter paper and the concentration of the filtrate was measured using a UV-vis spectrophotometer (Labtronics, LT-2204, India) at 665 nm. The adsorption capacity (Q_e) and dye removal were calculated using Equations 1 and 2.

$$Q_e(mg/g) = \frac{(C_e - C_o) \times 0.1}{W} \tag{1}$$

$$\% \text{ dye removal} = \frac{C_e - C_o}{C_o} \times 100 \tag{2}$$

C_o = initial concentration of MB before adsorption (ppm), C_e = final concentration of MB after adsorption (ppm), W = weight of the SCSW (g)

2.4 Designing of Experimental Runs

The DoE approach was used to find the systematic relationship between independent and dependent variables affecting the adsorption process. Two stages of

DoE approaches were being adopted in this adsorption study. In the 1st stage, screening design was used, followed by RSM methodology (hybrid-DoE), where central composite design was employed. The Quantum XL 14.0 software is used to design experimental runs.

2.4.1 Screening Design

There are several parameters affecting the adsorption process, and a few of them have little to no impact. Manually varying each parameter to examine its impact on the process takes a lot of effort and is not cost-effective. To find out the most influencing parameters and their interactions with other potential parameters, screening designs are utilized (Sharif et al., 2014). The operating parameters considered for screening and their ranges were reaction temperature (30–80 °C), pH (3–10), reaction time (20–120 min), initial concentration of dye (20–100 ppm), adsorbent dose (0.1–1 g/100 ml), and RPM (100–250). A total of 14 experimental runs were predicted through screening design, as reported in Table 1 while considering adsorption capacity and dye removal as response parameters.

2.4.2 Optimization Design

In order to optimize the impact of an individual and interacting effects of input variables on responses, 5 factor-5 level CCD was employed to experimental designs. Based on the results of screening design, experimental runs were designed with reduced operating parameters (least influential parameter is kept constant) for optimization study as shown in Table 2. Reaction time was fixed for 120 min whereas reaction temperature (30–90 °C), pH (3–10), initial dye concentration (10–95 ppm), adsorbent dose (0.75–2.25 g/100 ml), and RPM (75–225) were varied while adsorption capacity and dye removal were selected as responses. A total of 50 experimental runs were recommended by full factorial CCD (α=2.38), tabulated in Table 2.

It was to be noticed that 9 extra runs were also given in Table 2 under the manual optimization heading, which were manually designed and performed after analyzing the results of optimization runs (50 runs). The retrofitting of these nine additional experimental runs was done to get actual

Table 1 Designing of experimental runs for the adsorption using screening design

Run	Temp (°C)	pH	Time (min)	Dye conc. (ppm)	Adsorbent dose (g/100 ml)	RPM	Adsorption capacity (mg/g)	Dye removal (%)
1	80	3	120	100	0.1	100	5.84	22.45
2	30	10	120	100	0.1	250	24.42	93.88
3	30	3	20	100	0.1	100	8.20	31.53
4	80	10	120	20	1	250	5.82	96.05
5	30	10	20	20	1	250	5.45	90.00
6	80	3	120	100	1	250	22.88	87.95
7	30	3	120	20	1	100	5.51	91.63
8	30	10	20	100	1	100	18.38	70.64
9	80	10	120	100	1	100	23.65	90.89
10	30	10	20	20	0.1	100	5.62	92.74
11	80	10	20	100	0.1	250	18.10	69.47
12	80	3	120	20	0.1	250	2.13	35.21
13	80	3	20	20	1	100	5.03	83.02
14	30	3	20	20	0.1	250	3.63	59.91

response maxima that the proposed optimization runs could not provide. In optimization study, the optimum point is the point where the response value is close to desired value as in the present case, maximizing the response is desired. The main effect plots of all input variables should follow an asymptotic trend and the maximum point should be considered optimum point for the input variable. In the present study, an asymptotic trend was not obtained with the chosen range of input variables; hence, additional runs were performed by taking the values outside the range. This design is named hybrid optimization design (DoE + manual). All the experiments were performed in triplicate, and average values are used for analysis.

2.5 Isotherms, Kinetics, and Thermodynamic Studies

Adsorption isotherms are primarily employed to elucidate the interaction mechanism between the absorbent and adsorbate, determining whether the adsorption process is monolayer or multilayer, and whether it involves chemical or physical interactions (Al-Ghouti & Da'ana, 2020). In this study, 2-parameter isotherm models (Langmuir, Freundlich, Temkin, and Dubinin-Radushkevich adsorption isotherms) were used to study MB-SCSW isotherms at different temperatures (30 °C, 40 °C, 50 °C, and 60 °C) (Al-Ghouti & Da'ana, 2020;

Ali et al., 2021; Maruthapandi et al., 2018). Four different kinetic models were used to study MB-SCSW kinetics at different MB dye concentrations (40, 70, 120, and 150 ppm) at fixed temperature (50 °C), and pH (6.5). These kinetic models are pseudo-first-order, pseudo-second-order, Elovich kinetic, and intraparticle diffusion model. To comprehend the adsorption process's nature, thermodynamic favorability was checked and thermodynamic factors ($\Delta G°$, $\Delta H°$, and $\Delta S°$) were calculated (Zhu et al., 2018).

2.6 Regeneration and Reutilization Study

For regeneration of dye-adsorbed SCSW, chemical and thermochemical regeneration techniques were used adopted from the literature (Momina & Suzylawati, 2020). In thermo-chemical regeneration technique, the dye-adsorbed SCSW samples were heated at 100 °C for 2 h to loosen the bond between SCSW and MB. Furthermore, thermally treated SCSW was chemically treated using 0.1 M HCl for 2 h to leach loosely held MB onto the SCSW surface. On the other hand, in the chemical regeneration technique, MB-coated SCSW was only treated with 0.1 M HCl for 2 h. Both chemically and thermo-chemically regenerated SCSW samples were further used for adsorption experiments to carry out lifecycle assessment of SCSW with initial dye concentration of 20 ppm at 50 °C.

Table 2 Designing of experimental runs for the optimization study

Run	Temp	pH	Dye conc.	Ads. dose	RPM	Ads. capacity	Dye removal
1	80	4	25	2	200	1.65	97.3
2	40	4	25	2	100	1.65	97.2
3	40	4	80	2	200	4.55	95.4
4	80	9	25	1	100	3.17	93.5
5	60	6.5	53	1.5	150	3.99	97
6	80	4	25	1	100	3.25	95.8
7	60	6.5	53	1.5	150	3.99	97
8	80	9	25	1	200	3.28	96.7
9	60	6.5	53	1.5	150	3.99	97
10	40	9	80	1	200	9.26	97.1
11	40	4	80	1	100	8.92	93.5
12	60	6.5	53	2.25	150	2.61	97.4
13	40	4	80	1	200	9.12	95.5
14	80	9	80	2	100	4.62	96.9
15	40	4	25	1	200	3.27	96.3
16	40	9	25	2	200	1.65	97.6
17	40	9	25	2	100	1.64	96.9
18	40	9	80	1	100	9.16	96
19	60	3	53	1.5	150	3.93	95.7
20	80	9	25	2	200	1.65	97.6
21	80	4	25	1	200	3.26	96.1
22	80	9	25	2	100	1.63	96.4
23	80	9	80	1	100	9.06	95
24	60	6.5	53	1.5	150	3.93	95.7
25	30	6.5	53	1.5	150	3.94	96
26	40	4	25	2	200	1.65	97.6
27	60	10	53	1.5	150	3.99	97.2
28	80	9	80	2	200	4.65	97.4
29	60	6.5	53	0.75	150	7.83	95.2
30	80	9	80	1	200	9.12	95.6
31	40	4	80	2	100	4.6	96.4
32	40	9	25	1	100	3.26	96.1
33	60	6.5	53	1.5	75	3.96	96.3
34	40	9	80	2	100	4.64	97.2
35	60	6.5	53	1.5	225	3.97	96.6
36	40	4	25	1	100	3.28	96.7
37	40	9	80	2	200	4.64	97.2
38	60	6.5	10	1.5	150	0.65	95.4
39	80	4	80	2	100	4.61	96.8
40	40	9	25	1	200	3.3	97.2
41	80	4	80	2	200	4.64	97.3
42	60	6.5	53	1.5	150	3.99	97
43	80	4	80	1	200	9.11	95.5
44	80	4	80	1	100	9.03	94.6
45	60	6.5	53	1.5	150	3.99	97
46	80	4	25	2	100	1.63	96.4
47	60	6.5	53	1.5	150	3.99	97

Table 2 (continued)

Run	Temp	pH	Dye conc.	Ads. dose	RPM	Ads. capacity	Dye removal
48	60	6.5	95	1.5	150	5.48	96
49	60	6.5	53	1.5	150	3.99	97
50	90	6.5	53	1.5	150	3.96	96.2
Manual optimization runs							
51	60	11	52.5	1.5	150	5.34	97.55
52	60	12	52.5	1.5	150	5.25	96.04
53	60	6.5	52.5	0.5	150	14.12	86.05
54	60	6.5	52.5	0.2	150	35.87	87.41
55	60	6.5	52.5	2.5	150	3.23	98.31
56	60	6.5	52.5	0.1	150	71.49	87.11
57	60	6.5	150	0.1	150	96.27	61.18
58	60	6.5	200	0.1	150	164.47	65.83
59	60	6.5	105	1.5	150	8.19	91.73

Table 3 % contribution of operating parameters

Term	Adsorption capacity (mg/g)			% Dye removal		
	SE	SS	% Contribution	SE	SS	% Contribution
A, temperature	−1.48	5.84	0.74	−9.19	225.08	2.76
B, pH	4.16	46.09	5.88	25.21	1694.2	20.77
C, time	1.92	9.88	1.26	7.32	143.05	1.75
D, dye conc.	13.66	497.90	63.48	−10.81	311.75	3.82
E, SCSW dose	4.59	56.16	7.16	26.62	1890.2	23.17
F, RPM	3.47	32.13	4.10	6.33	106.96	1.31

SE standardized error, *SS* sum of squares

3 Results and Discussions

3.1 Screening Design

All the experiments reported in Tables 1 and 2 were carried out using batch adsorption and responses (adsorption capacity and dye removal) are also provided in Table 1. Table 3 lists the contributions of the input parameters for both responses. It can be seen that reaction time seems to least influential parameter that may be held constant for optimization study to maximize the adsorption of dye onto SCSW, as shown by the % contribution values (1.26 and 1.75%). It is to be noted that dye concentration (63%) and adsorbent dosage (23%) are the factors having the greatest influence on adsorption capacity and dye elimination.

3.2 Optimization Studies

The experimental runs suggested by the Quantum XL (initial 50 runs in Table 2) were performed and output responses are inserted into the DOE module to perform the regression analysis. The coefficient of regression (R^2) of adsorption capacity and dye removal is found to be 0.99 and 0.90, respectively, indicating well-fitting of the adsorption capacity response compared to the dye removal response. The second-order quadratic equations for both dye removal and adsorption capacity derived from the regression analysis are given in Eq. (3 & 4). The ANOVA for both responses is given in Table S-1 of supplementary material. In the adsorption capacity regression model, it is to be noted that linear terms as well as multiplied terms of dye concentration (C) and SCSW dose (D) are more significant compared to other input variables, because

the *p*-value of C, D, CC, and DD is less than 0.05. In contrast, the linear terms of pH (B), dye concentration (C), adsorbent dose (D), RPM (E), and interactive terms AB, AC, AD, BC, DE, BCDE, having *p*-values less than 0.05, are more significant for the dye removal regression model.

The regression analysis was again carried out after the incorporation of manual optimization runs (as explained in Section 2.3.3), totaling 59 runs. A slight reduction in R^2 of adsorption capacity, i.e., 0.96 is noticed; however, R^2 of dye removal remains constant, i.e., 0.90, both under the acceptable range, indicating the well-fitting of the model. The regression equation for hybrid design is given in Eqs. (5 and 6) whereas ANOVA results for hybrid design are given as Table S-2 in supplementary file.

$$
\begin{aligned}
\text{Adsorption capacity} = {} & 3.8709 - 0.0791A + 0.0305B + 2.1303C - 2.3228D + 0.0177E - 0.0297AB \\
& + 0.0051AC + 0.0204AD + 0.0027AE + 0.034BC - 0.0214BD + 0.0034BE \\
& - 0.1718CD + 0.0091CE - 0.0272DE - 0.0227ABC + 0.027ABD + 0.0041ABE \\
& + 0.0064ACD - 0.0066ACE + 0.0122ADE - 0.0243BCD - 0.0106BCE + 0.0002BDE \\
& - 0.0192CDE + 0.0131ABCD - 0.0006ABCE - 0.0166ABDE + 0.0192ACDE \\
& + 0.0229BCDE - 0.0061ABCDE - 0.182A^2 + 0.2715B^2 - 0.2789C^2 + 1.5315D^2 - 0.1236E^2
\end{aligned}
\tag{3}
$$

$$
\begin{aligned}
\%\text{Dye removal} = {} & 96.664 - 0.0909A + 0.4236B - 0.2458C + 0.8995D + 0.3088E - 0.4314AB + 0.2573AC \\
& + 0.3615AD + 0.1638AE + 0.4645BC - 0.0937BD + 0.2127BE + 0.138CD - 0.0612CE \\
& - 0.2825DE - 0.2682ABC + 0.3313ABD + 0.0583ABE + 0.0583ACD - 0.1326ACE \\
& + 0.1049ADE - 0.1994BCD - 0.2222BCE - 0.0599BDE - 0.2307CDE - 0.1221ABCD \\
& - 0.1049ABCE - 0.2616ABDE + 0.3148ACDE + 0.4227BCDE - 0.0174ABCDE \\
& - 0.1761AA + 0.097BB - 0.292CC - 0.053DD + 0.0434EE
\end{aligned}
\tag{4}
$$

$$
\begin{aligned}
\text{Adsorption capacity} = {} & 0.6807 - 0.9956A + 0.4366B - 1.945C - 4.409D + 0.0177E - 0.0297AB \\
& + 0.0051AC + 0.0204AD + 0.0027AE + 0.034BC - 0.0214BD + 0.0034BE \\
& - 1.8877CD + 0.0091CE - 0.0272DE - 0.227ABC + 0.027ABD + 0.0041ABE \\
& + 0.0064ACD - 0.0066ACE + 0.0122ADE - 0.0243BCD - 0.0106BCE \\
& + 0.0054BDE - 0.0192CDE + 0.0131ABCD - 0.0006ABCE - 0.0166ABDE \\
& + 0.0192ACDE + 0.0229BCDE - 0.0061ABCDE - 2.5249AA + 0.7889BB \\
& + 2.8817CC - 10.797DD - 1.6153EE
\end{aligned}
\tag{5}
$$

$$
\begin{aligned}
\%\text{Dye removal} = {} & 96.626 - 0.3602A + 0.3511B - 0.6735C + 1.7093D + 0.3088 - 0.4314AB + 0.2573AC \\
& + 0.3615AD + 0.1638AE + 0.4645BC - 0.0937BD + 0.2127BE + 1.4392CD - 0.0612CE \\
& - 0.2825DE - 0.2682ABC + 0.3313ABD + 0.0583ABE + 0.0583ACD - 0.1326ACE \\
& + 0.1049ADE - 0.1994BCD - 0.2222BCE - 0.0599BDE - 0.2307CDE - 0.1221ABCD \\
& - 0.1049ABCE - 0.2616ABDE + 0.3148ACDE + 0.4227BCDE - 0.0174ABCDE \\
& + 0.5023AA + 0.1244BB - 0.1907CC - 2.394DD + 0.4792EE
\end{aligned}
\tag{6}
$$

Table 4 Comparison of optimum conditions obtained from DoE and hybrid design.

Input parameters	DoE-CCD		Hybrid-design (DoE +manual)	
	Adsorption capacity	Dye removal	Adsorption capacity	Dye removal
Temperature (°C)	30	30	57	30
pH	10	2.8	12	12
Dye conc. (ppm)	95	10	200	200
Adsorbent dose (g)	0.75	2.25	0.1	2.5
RPM	225	225	150	105
Response (Pred.)	13.17 mg/g	98.75%	162.12 mg/g	100%
Response (Exp.)	15.29 mg/g	95.91%	246.45 mg/g	97.70%

Fig. 1 Effect of **a** temperature on adsorption capacity (12 pH, 200 ppm, 0.1 g, 150 RPM) and dye removal (12 pH, 200 ppm, 2.5 g, 105 RPM); **b** pH on adsorption capacity (57°C, 200 ppm, 0.1 g, 150 RPM) and dye removal (30 °C, 200 ppm, 2.5 g, 105 RPM); **c** pH_{pzc} of SCSW; **d** adsorbent dose on adsorption capacity (57°C, 12 pH, 200 ppm, 150 RPM) and dye removal (30 °C, 12 pH, 200 ppm, 105 RPM); **e** dye concentration on adsorption capacity (57°C, 12 pH, 0.1 g, 150 RPM) and dye removal (30 °C, 12 pH, 2.5 g, 105 RPM); **f** RPM on adsorption capacity (57°C, 12 pH, 200 ppm, 0.1 g) and dye removal (30 °C, 12 pH, 200 ppm, 2.5 g)
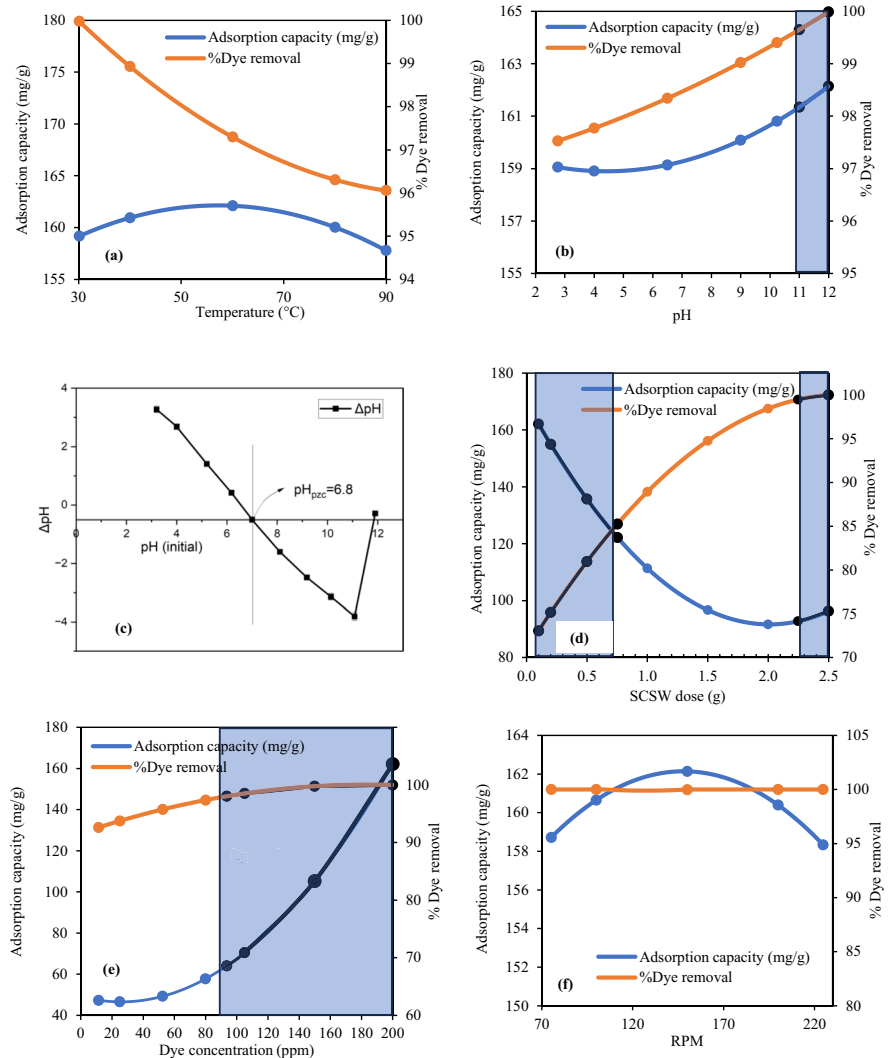
3.3 Optimization of Parameters

Based on the regression analysis performed by Quantum XL, optimization of both designs (DoE and hybrid design) was carried out by keeping maximization of adsorption capacity and dye removal as a set objective. Optimized conditions and respective response values for DoE and hybrid designs are compared in Table 4. It can be seen that the optimized conditions are substantially different, and by including extra runs in the DoE design, adsorption capacity is enhanced by a factor of more than 10 (13, to be précised). The removal of dye is also improved a little bit, and MB is shown to be eliminated entirely (100%). Additionally, experimental runs are performed under optimal circumstances, and results are similar to those predicted, as shown in Table 4. Hence, it is evident that hybrid design produces better results in comparison to DoE alone and will be considered further to generate other results. The influence of input parameters (individual as well as interaction) was carried out by varying one/two parameters at a time and keeping others fixed. The values of the fixed parameters are maintained at their optimized levels, which are listed in Table 4.

3.3.1 Main Effect of Individual Parameter

Main effect plots, in Fig. 1, present the influence on responses (adsorption capacity and dye removal) by varying the input variables. The extra runs performed for hybrid design are presented with shaded areas in the main effects plots.

The influence of temperature (A), presented in Fig. 1(a), was studied by varying temperature from 30 to 90°C while other parameters are fixed at optimized levels to maximize the adsorption capacity (pH =12, dye concentration = 200, SCSW dose =0.1 g, RPM =150 rpm) and dye removal (pH =12, dye concentration=200 ppm, SCSW dose =2.5 g, RPM=105 rpm). Figure 1(a) illustrates that the adsorption capacity increases until 60°C before it begins to decline again; however, on the other hand, the dye removal falls constantly as the temperature rises. An increase in temperature enhances the mass transfer rate, so the adsorption capacity increases, whereas the dye removal capability reduces with increasing temperature due to the exothermic nature of the adsorption (Mansour et al., 2021). In later sections, the effect of

temperature is vividly explained through adsorption thermodynamic analysis.

Figure 1(b) represents the effect of pH on adsorption capacity and dye removal. It is seen that there is an increment in adsorption capacity and dye removal with an increase in pH from 3 to 10 but no asymptotic value is attained. Therefore, two further runs are carried out at pH 11 and 12, referred as runs 51 and 52 in Table 2, where further increase in adsorption capacity and dye removal is noticed. At higher pH values, deprotonation of the adsorbent surface takes place, resulting in the electrostatic interaction of the cationic MB dye molecule with the adsorbent surface. This is justified by pH_{pzc} of SCSW, i.e., 6.8, illustrated in Fig. 1(c). If the pH of the solution is greater than pH_{pzc}, the SCSW surface becomes more negatively charged, attracting more cationic species (MB dye molecules) to the surface and resulting in a deprotonation mechanism that increases adsorption capacity and dye removal (Sahu et al., 2020), since the pH_{pzc} provides the information on ionization of functional groups and the nature of interactions between H^+ and OH^- in the dye solution (Iheanacho et al., 2023). The surface of SCSW contains various functional groups attributed to the presence of bio-polymers such as cellulose, hemicellulose, and lignin (Modak et al., 2023). With the solution's pH, the concentration of hydroxyl ions (OH^-) rises, causing protons to be drawn from the surface functional groups of SCSW. These protons then combine with hydroxyl ions to form water (H_2O). The electron-rich functional groups on the surface of SCSW become favorable sites for the adsorption of cationic species (MB). When the solution's pH exceeds the pHpzc of SCSW (6.8), deprotonation accelerates, leading to an increased efficiency in dye removal (Iqbal et al., 2019).

Figure 1(d) illustrates that as the adsorbent dose is increased from 0.75 to 2.25 g, the adsorption capacity decreases, while dye removal increases. To further investigate the impact of extreme values of SCSW dose, four additional runs were conducted at SCSW doses of 0.1, 0.2, 0.5, and 2.5, denoted as runs 53–56 in Table 2 and shaded areas in Fig. 1(d). It is noteworthy that the adsorption capacity reaches its peak at the lowest SCSW dosage of 0.1 g, but the highest dye removal occurs at the highest SCSW dose of 2.5 g. At a constant dye concentration (200 ppm), an increase in the adsorbent dose leads to a decrease in adsorption capacity due to the saturation of active sites or an

increase in the number of available active sites. However, with a higher adsorbent dosage, more dye molecules bind to the SCSW adsorbent, facilitated by an increased number of active and accessible adsorption sites (Subramani & Thinakaran, 2017).

Figure 1(e) showcases the effect of dye concentration on adsorption capacity as well as dye removal. With an increment in dye concentration, the adsorption capacity increases abruptly from 10 to 95 ppm due to the increase in dye molecules for the fixed number of active sites present in SCSW, leading to a higher adsorption rate. Similarly, the dye removal also gets slightly enhanced with an increase in dye concentration due to reduction in mass transfer resistance between the SCSW surface and the MB dye molecule (Iqbal et al., 2019). To further investigate the effect of dye concentration at higher values, three extra runs are carried out at dye concentrations of 105, 150, and 200 ppm, which shows that adsorption capacity and dye removal are enhanced at higher concentration as well. These extra runs are given as runs 57–59 in Table 2 and with shaded areas in Fig. 1(e). Hence, it can be perceived that even with a small amount of SCSW, dye solutions of high concentration can also be treated and optimized value for dye concentration is found to be 200 ppm for both the responses.

Figure 1(f) illustrates the impact of RPM on adsorption capacity and dye removal. There is no significant change observed in dye removal with an increase in RPM; however, the adsorption capacity increases with RPM until 150 RPM. This is attributed to an increase in turbulence, causing a reduction in the boundary layer thickness around the surface of the adsorbent. Beyond 150 RPM, the adsorption capacity decreases, suggesting a possibility that excessive collisions between the adsorbent at higher RPM may lead to desorption, resulting in a reduction in adsorption capacity (Kheddo et al., 2020).

3.3.2 Effect of Interaction of Multiple Variables

In the above section, the effects of individual parameters on the responses are presented; however, interaction of input parameters also greatly affects the responses. The study of the interaction of input parameters in the due process of adsorption can be carried out using DoE, as provided in Fig. S-1 to Fig. S-10. The interaction between temperature and pH can be seen in Fig. S-1.1; dye removal is increasing with pH at low temperatures (30–60 °C) and decreasing at high temperatures (60–90°C). This indicates a clear interaction effect of temperature and pH where individual effects are diluted, as explained in the main effect section. The maximum dye removal is observed at two points: (1) low temp and high pH (30 °C, 12 pH) high temp and low pH (90 °C, 2.7 pH). However, the saddle behavior is observed in adsorption capacity as shown in Fig. S-1.2, where maximum adsorption capacity is increased until 60 °C and again reduced until 90 °C; however, adsorption capacity is continuously increased with pH. It is noteworthy that both temperature and pH are depicting their individual effects only, as shown in main effects plot, and the interaction of both parameters does not have any discernible impact on the adsorption capacity. Maximum adsorption capacity is found at 57 °C and 12 pH similar to the main effect values. In Fig. S-2.1, dye removal is pretty much influenced by the temperature and dye concentration interaction. At low temperatures (30 °C), dye removal increases with dye concentration. However, when temperature is also increased with concentration, dye removal is first increased then decreased resulting in the shifting of maxima toward the higher temperature and lower concentration. In the case of adsorption capacity plot (Fig. S-2.2), individual effects of temperature and concentration are retained as adsorption capacity is increased until 57 °C and then decreased for all dye concentration levels. Dye removal is increased exponentially with an increase in dye concentration at all temperatures; hence, maxima would be attained at highest concentration (200 ppm) and 57°C.

In Fig. S-3.1, the dye removal is increased with temperatures at low adsorbent doses from 0.1 to 1.12 g, then starts decreasing until 2.5 g. Therefore, an interaction effect is easily identifiable due to the fact that dye removal should go down with temperature and up with dosage, in accordance with individual effects. In terms of adsorption capacity, shown in Fig. S-3.2, the temperature and dose hold their individual effects when only one parameter is varied, as explained in main effect section. However, when temperature and dose varied simultaneously, their interaction effect is dominated by the adsorbent dose effect and adsorption capacity decreases up to 2 g then starts increasing with an increase in both parameters.

In Fig. S-4.1, low temperature and RPM result 100% dye removal and no significant variation is

observed with increasing RPM; however, as temperature rises, dye removal declines due to the individual effect of temperature. This reduction in dye removal is compensated by increasing the RPM simultaneously, resulting in 100% dye removal at higher temperatures and RPM. On the other hand, the temperature and RPM interaction produce a dome-shaped response for adsorption capacity, where the maxima are obtained at the points, i.e., 57 °C and 150 rpm as shown in Fig. S-4.2.

The interaction between pH and dye concentration, as shown in Fig.S-5.1, leads to enhancement in dye removal as well as adsorption capacity with an increase in both parameters by retaining their individual effects. Nevertheless, the adsorption capacity remains relatively unaffected by changes in pH, whereas the adsorption capacity experiences a significant rise with higher concentrations of dye, thus resulting in concave upward behavior as shown in Fig. S-5.2. The interactions between pH and adsorbent dosage, shown in Fig. S-6.1, indicate that the removal of dye is improved as a result of the positive influence of both parameters on the dye removal. The interaction of adsorbent dose and pH, given in Fig. S-6.2, showcased that the adsorbent dose effect is more pronounced than the pH effect, resulting in a

Fig. 2 Linear adsorption isotherm models of MB dye adsorption onto SCSW at different temperatures (dose=0.2 g, pH=6.5, RPM=150, time=120 min) **a** Langmuir, **b** Freundlich, **c** Temkin, **d** Dubinin-Radushkevich, **e** separation factors with different dye concentrations
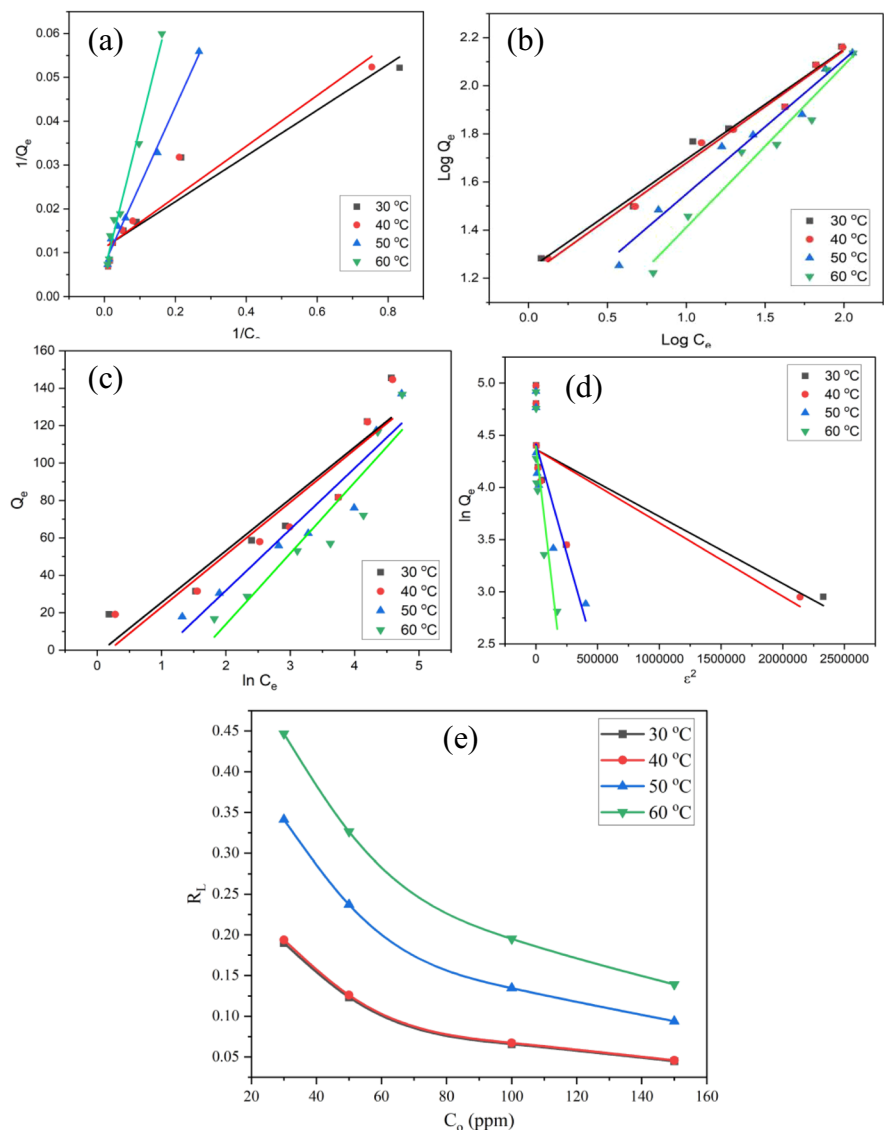
Table 5 Parameters of adsorption isotherms and kinetic analysis: linear adsorption isotherms parameters at various temperatures

	Temperatures (°C)			
	30	40	50	60
Linear Langmuir absorption isotherm model				
Q_{max} (mg/g)	89.20	90.17	134	168.06
K_L (L/mg)	0.214	0.191	0.041	0.018
R^2	0.916	0.925	0.990	0.984
Linear Freundlich adsorption isotherm				
$1/n$	0.457	0.467	0.560	0.674
K_f ((mg/g) (L/mg)$^{1/n}$)	17.221	16.282	9.751	5.449
R^2	0.982	0.988	0.971	0.964
Linear Temkin adsorption isotherm				
B (J/mol)	27.65	28.06	32.71	37.93
b_T	91.08	92.72	82.07	72.98
A_T (L/g)	0.924	0.832	0.358	0.194
R^2	0.886	0.886	0.913	0.870
Linear Dubinin-Radushkevich adsorption isotherm				
Q_{max} (mg/g)	78.74	78.56	82.95	53.89
K_d (mol/J) ($\times 10^{-6}$)	0.64	0.70	4.21	14.4
E (KJ/mol)	0.81	0.84	0.34	0.18
R^2	0.597	0.603	0.767	0.730

*Q_t, amount of dye uptake at time t

concave downward surface plot for adsorption capacity. As shown in Fig. S-7.1, the pH and RPM have a noteworthy interaction impact on dye removal; an increase in RPM causes a considerable decline in dye removal at low pH but no significant difference is seen at higher pH. In contrast, at lower RPM, dye removal is almost constant but increases at higher RPM with increasing pH. In addition, when both RPM and pH are increased simultaneously, dye removal is first declining then starts increasing, giving maxima at two points, i.e., (i) any pH and 75 RPM and (ii) 12 pH and any RPM. In Fig. S-7.2, a saddle-type response is found, maintaining the individual effects of pH and RPM on adsorption capacity as explained in main effect section.

The interaction between dye concentrations and adsorbent dose, given in Fig. S-8.1, shows that at low adsorbent dose upto 1.8 g, dye removal declines with concentration however improved at higher doses. With simultaneous increase in concentration and dose, dye removal first rises, then drops to 105 ppm and continuously rises for higher concentrations. In

Fig. S-8.2, it is evident that the individual effects of both parameters on adsorption capacity are followed; however, simultaneous increase in concentration and dose result a decrease in dye removal, reaching a minimum at 43 ppm and 1.6 g before rising again.

The interaction plots between dye concentration and RPM, given in Fig. S-9.1 and S.-9.2, show a typical concave downward trend for dye removal and adsorption capacity, indicating the dominance of the concentration effect on the RPM effect. The dye removal is enhanced due to an increase in dye concentration at all levels of RPM. Similarly, interaction plots of adsorbent dose and RPM show the pronounced effect of dose over that of RPM as shown in Fig. S-10.1 and S-10.2.

3.4 Isotherms, Kinetics, and Thermodynamic Studies

3.4.1 Adsorption Isotherms

Figure 2(a–d) depicts the adsorption isotherm plots obtained from the fitting of linear adsorption isotherms with experimental data at various temperatures, and goodness-of-fit and constants are given in Table 5. For Langmuir adsorption, isotherms of all temperatures fit well as indicated by R^2 (0.99> R^2>0.916) whereas they show best fitting at 50 °C (R^2 ~0.99) as illustrated in Fig. 2(a). Figure 2(e) illustrates the variation of the separation factor (R_L) with C_o, highlighting the favorable adsorption process since R_L is less than 1 for all temperatures. At low initial dye concentrations, however, the adsorption process becomes even more favorable (Khan et al., 2018). Freundlich isotherms also provide the good fitting (0.98> R^2 >0.96) in all adsorption temperatures and fits best at 40 °C (R^2~0.98). With an increase in temperatures (30–40 °C) and (50–60 °C), the $1/n$ value decreases, resulting in heterogeneous adsorption of MB onto SCSW (Al-Ghouti & Al-Absi, 2020). As mentioned in section 2.5.1, Langmuir's adsorption isotherm indicates the monolayer coverage of homogeneous adsorbent surface whereas Freundlich's adsorption isotherm represents the adsorption onto the heterogeneous surface of adsorbent.

This indicates that MB dye molecules are positively competing for both monolayer and multilayer coverage at the homogeneous and heterogeneous adsorption sites of SCSW. Temkin isotherm also accounts for adsorbate and adsorbent interaction; at

Fig. 3 Adsorption kinetics analysis. **a1** Kinetics of adsorption (temp=50 °C, pH=6.5, dose=0.2 g, RPM-150). **a2** UV-vis spectra of the dye removal at different times (C_o=150 ppm, temp=50 °C, pH=6.5, dose=0.2 g, RPM-150). **b** Non-linear kinetic adsorption models at different initial dye concentration (temp=50 °C, pH=6.5, dose=0.1 g, RPM=150) **b1** 40 ppm, **b2** 70 ppm, **b3** 120 ppm, **b4** 150 ppm
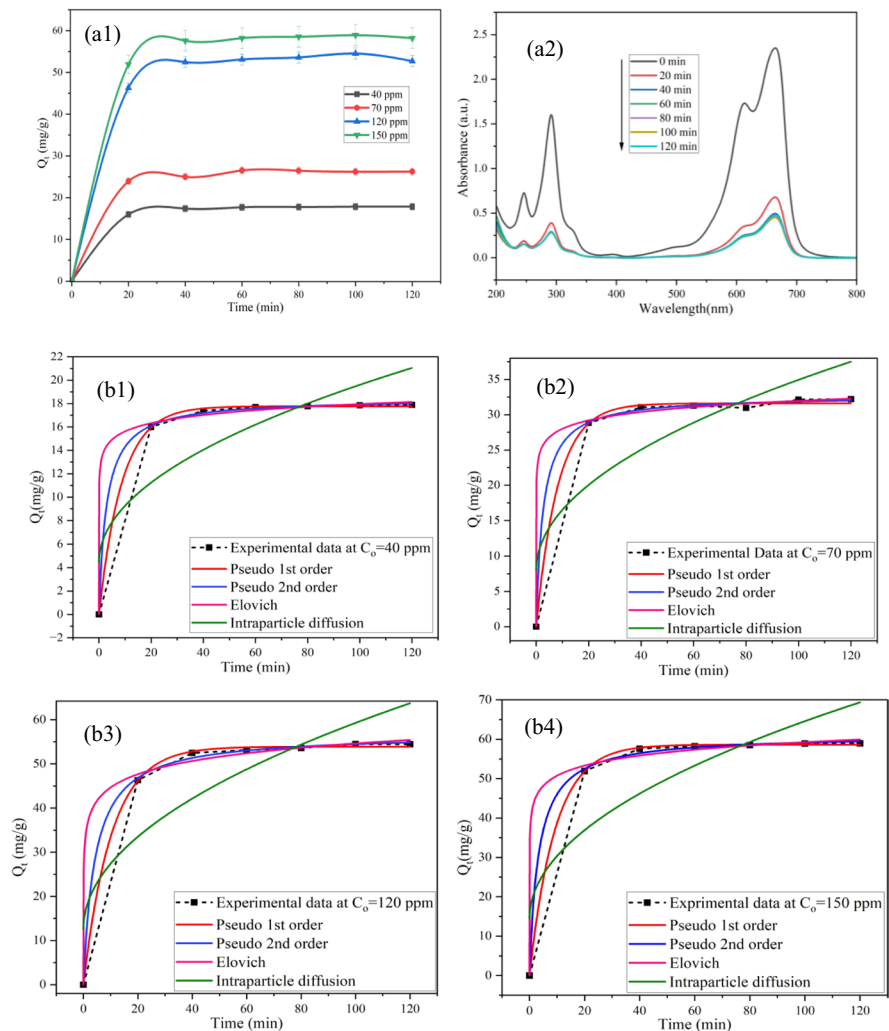
50 °C, the model shows a better fitting compared to other temperature, i.e., ~0.91 and A_T values decrease with increasing temperatures, implying the adsorption process to be exothermic in nature (Aljeboree et al., 2017). Dubinin-Radushkevich (D-R) adsorption isotherms show weak fitting compared to Langmuir, Freundlich, and Temkin isotherm models. Q_{max} calculated by the D-R model is maximum at 50 °C having the maximum R^2~0.767 in comparison to other temperatures. The E values for all the temperatures are less than 8 kJ/mol which indicates that the adsorption process is physisorption, in good accord with the Temkin isotherm (Sahoo & Prelot, 2020). It is to be observed that a good adsorbent characteristic is exhibited by SCSW at 50 °C (Q_{max} and R^2 are

maximum) compared to other temperatures and all the isotherm models are well fitted.

3.4.2 Kinetic Analysis

Figure 3(a1) and (a2) shows that the SCSW attains the equilibrium in 40 min for all initial dye concentrations; however, with an increase in initial dye concentrations, the dye uptake (Q_t) increases. High dye concentration leads to a higher mass transfer gradient, which in turn leads to an increase in the driving force between MB molecules and SCSW resulting in maximum amount of MB molecules uptake (Basha et al., 2022). In Fig. 3(a2), the UV-vis spectrogram illustrates dye removal at different time with λ_{max} at ~665

Table 6 Parameters of adsorption isotherms and kinetic analysis: non-linear kinetic model parameters

	Initial dye concentration (ppm)			
	40	70	120	150
Q_e (mg/g) (experimental)	17.88	33.0	55.8	59.0
Pseudo-first-order kinetic model $Q_t = Q_e\left(1 - e^{-k_1 t}\right)$				
Q_e (mg/g) (calculated)	17.769	31.5953	53.9184	58.638
K_1 (1/min), rate constant	0.11421	0.12054	0.097	0.10785
Chi-square	0.01258	0.24872	0.25333	0.07647
R^2	0.99976	0.99851	0.99947	0.99987
Pseudo-second-order kinetic model $Q_t = \frac{Q_e^2 k_2 t}{1 + Q_e k_2 t}$				
Q_e (mg/g) (calculated)	18.436	32.708	56.8041	61.0814
K_2 (g/mg min), rate constant	0.0188	0.01161	0.00413	0.0050
Chi-square	0.01651	0.15098	0.37361	0.40475
R^2	0.99969	0.9991	0.99922	0.99987
Elovich kinetic model $Q_t = \frac{1}{\beta} \ln\left(1 + \alpha\beta t\right)$				
β (mg/g), adsorption constant	0.9865	0.58055	0.23093	0.27037
α (mg/g min), desorption constant	498494.70	1969250.3	13045.13	335659.3
Chi-square	0.07724	0.20821	1.31672	1.33419
R^2	0.99853	0.99875	0.99726	0.99766
Intraparticle diffusion kinetic model $Q_t = K_{diff} t^{0.5} + C$				
K_{diff} (mg/g.min$^{0.5}$), diffusion rate coefficient	1.5112	2.6937	4.6634	5.0071
C (mg/g), thickness of the boundary layer	4.4756	7.99618	12.653	14.5161
Chi-square	13.83854	44.04197	111.81	146.307
R^2	0.73704	0.73638	0.76725	0.74393

*Q_t, amount of dye uptake at time t

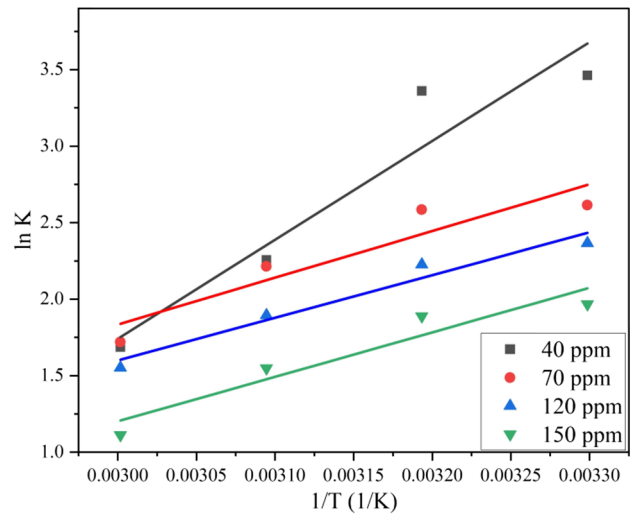**Fig. 4** Plot of lnK vs 1/T for thermodynamic analysis

Table 7 Thermodynamic parameters at various dye concentration

MB conc. (ppm)	$\Delta G°$ (kJ/mol)				$\Delta H°$ (kJ/mol)	$\Delta S°$ (J/mol. K)
	303 K	313 K	323 K	333 K		
40	−6.976	−6.942	−4.197	−2.752	−53.65	−152.33
70	−4.838	−4.924	−4.083	−2.844	−25.34	−66.56
120	−4.214	−3.990	−3.225	−2.378	−23.35	−61.96
150	−3.207	−3.111	−2.297	−1.160	−24.14	−68.24

nm. During the initial 20 min, there is a significant decrease in λ_{max} intensity from 2.3 to 0.7 a.u. Subsequently, over the next 20 min, a slight reduction in λ_{max} intensity from 0.7 to 0.5 a.u. is visible. Between 40 and 120 min, a minimal variation in the λ_{max} intensities indicates that SCSW reaches equilibrium within 40 min. Figure 3(b1–b4) depicts the fitting of nonlinear adsorption kinetic models with experimental data at different C_o (40,70,120,150 ppm) and kinetic evaluation is presented in Table 6.

It is interestingly demonstrated that the mechanism of MB adsorption onto SCSW involves both physisorption and chemisorption, as evidenced by R^2 values for pseudo-first-order and pseudo-second-order kinetic models close to 1 ($R^2 \sim 0.99$). At 40 ppm and 150 ppm, the chi-square values are the lowest, indicating that the calculated values of Q_e from the pseudo-first-order model are almost similar to the experimental values of Q_e at C_o=40 and 150 ppm, respectively. Similarly, at 40 and 70 ppm, the chi-square values are lower, suggesting that the calculated values of Q_e from the pseudo-second-order model are almost similar to the experimental values at 40 and 70 ppm. The Elovich model, referred to as the chemisorption model, fits very well at different MB initial dye concentrations ($R^2 \sim 0.99$). However, the chi-square value at 40 ppm is the lowest, indicating an appropriate fit of the Elovich model for 40 ppm. Intraparticle diffusion kinetics are not well-fitted, as implied by the low $R^2 \sim 0.7$ value and very high chi-square values for all concentrations, as given in Table 6. It can be inferred that intraparticle diffusion is not taking place in the MB-SCSW adsorption system.

3.4.3 Thermodynamic Analysis

Thermodynamic factors are calculated to check the favourability of adsorption process and are tabulated in**.** Thermodynamic factors ($\Delta G°$, $\Delta H°$, and $\Delta S°$) are calculated using the Eqs. 7, 8, and 9.
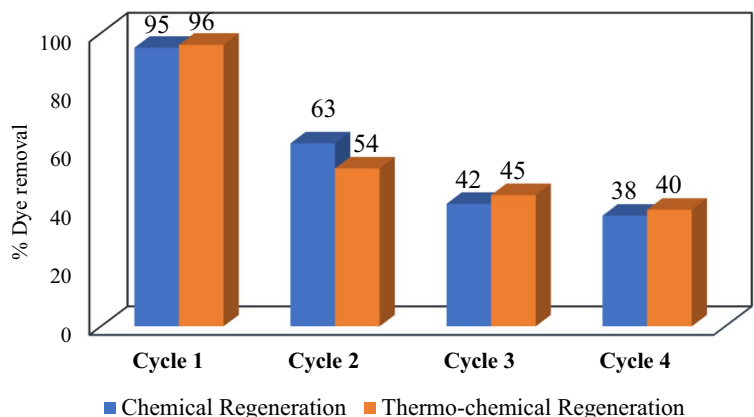
$$\Delta G° = -RT\ln K \tag{7}$$

$$K = \frac{Q_e}{C_e} \tag{8}$$

$$\ln K = -\frac{\Delta H°}{RT} + \frac{\Delta S°}{R} \tag{9}$$

where $\Delta G°$ = free energy change, $\Delta H°$ = change in enthalpy, $\Delta S°$ = change in entropy in Kelvin, and R =

Fig. 5 Regeneration cycles of chemically and thermochemically generated SCSW (C_o=20 ppm, temp= 50 °C, RPM=150, pH = 6.5, time = 2 h)

8.314 J/mol.K. The graph is plotted between ln K vs $1/T$, given as Fig. 4, slope and intercept are used to calculate $\Delta H°$ and $\Delta S°$ respectively (Al-Gorair et al., 2022).

It is noticeable that $\Delta G°$, $\Delta H°$, and $\Delta S°$ (Table 7) for all the variation in dye concentration and temperature are negative, depicting that MB adsorption process onto the SCSW surface is spontaneous and exothermic with less randomness. A trend could be noticed that there is a decrement in $\Delta G°$ with increase in temperature and dye concentration which highlights that the spontaneity is mildly reduced with increase in dye concentration and adsorption temperature. From 40 to 150 ppm, the adsorption process is a physical process as $\Delta H°$ is less than 40 kJ/mol and exothermic (Xu et al., 2018). The $\Delta G°$ falls into the range of physisorption which lies between the range of −20 to 0 kJ/mol for all the MB dye concentrations and temperatures. It could be concluded that the nature of the adsorption process is physical, exothermic, and spontaneous in nature. The negative values of $\Delta S°$ highlight a drop in instability of system at the solid/fluid boundary as temperature rises, i.e., the MB dye molecules display more organized layers on the adsorbent's surface (Gupta et al., 2011).

3.5 Regeneration and Reutilization of MB-Coated SCSW

The dye removal capability in each cycle for both chemically and thermochemically regenerated SCSW is represented in Fig. 5. In cycle 1, chemically and thermochemically regenerated SCSW result in effective dye removal, i.e., 95% and 96%, respectively; however, in cycle 2, dye removal drops significantly. Chemically regenerated SCSW shows a dye removal of 63% (~34% reduction compared to cycle 1), whereas the dye removal is 54% (~43% reduction from cycle 1) in thermochemically regenerated SCSW. In cycle 3, a further drop in dye removal is observed as chemically and thermochemically regenerated SCSW show a dye removal of 43% and 45% respectively. In cycle 4, both chemically and thermochemically regenerated SCSW exhibit dye removal of 38% and 40% respectively. Hence, it can be observed that in cycles 1 and 2, dye removal capability of chemically regenerated SCSW is better; however, dye removal capability of thermochemically regenerated SCSW is stable after cycle 2. In chemical regeneration, dilute acid only leaches the adsorbed MB out without any surface modifications, but in the thermochemical regeneration method, the surface modifications may take place by a slight increment of pores on SCSW, thus slightly enhancing the dye removal capability in the later cycles (Guo et al., 2020).

4 Conclusion

- In the present work, spent carrot seed waste (SCSW) was explored as an adsorbent for the exclusion of organic dyes such as MB from synthetic wastewater.
- SCSW exhibits excellent characteristics as an adsorbent, results in maximum adsorption capacity and dye removal of 246 mg/g and 98% through hybrid-DoE design.
- Isotherm results show that SCSW has both homogenous and heterogeneous surfaces where competitive monolayer coverage is taking place which is exothermic in nature.
- At 50 °C, Langmuir, Freundlich, and Temkin isotherm models are more suited, whereas in terms of kinetic analysis for MB-SCSW adsorption system, pseudo-first-order, pseudo-second-order, and Elovich models are highly applicable.
- Therefore, utilization of post-extraction carrot seed waste as a sustainable adsorbent can be an attractive, effective, and economic alternative to manage the solid waste and water waste generated by essential oil and textile industries respectively.

Declarations

Conflict of Interest   The authors declare no competing interests.

References

Abu Bakar, M. S., Ahmed, A., Jeffery, D. M., Hidayat, S., Sukri, R. S., Mahlia, T. M. I., et al. (2020). Pyrolysis of solid waste residues from Lemon Myrtle essential oils extraction for bio-oil production. *Bioresource Technology, 318*(June), 1–5. https://doi.org/10.1016/j.biortech.2020.123913

Al-Ghouti, M. A., & Al-Absi, R. S. (2020). Mechanistic understanding of the adsorption and thermodynamic aspects of cationic methylene blue dye onto cellulosic olive stones biomass from wastewater. *Scientific Reports, 10*(1). https://doi.org/10.1038/s41598-020-72996-3

Al-Ghouti, M. A., & Da'ana, D. A. (2020). Guidelines for the use and interpretation of adsorption isotherm models: A review. *Journal of Hazardous Materials, 393*(January), 122383. https://doi.org/10.1016/j.jhazmat.2020.122383

Al-Gorair, A. S., Sayed, A., & Mahmoud, G. A. (2022). Engineered superabsorbent nanocomposite reinforced with cellulose nanocrystals for remediation of basic dyes: Isotherm, kinetic, and thermodynamic studies. *Polymers, 14*(3). https://doi.org/10.3390/polym14030567

Ali, I., Khan, D., Mehmood, T., & Khan, A. (2021). Removal of Uranium U(IV) from aqueous solution using acid treated spent tea leaves. *Current Research in Green and Sustainable Chemistry, 4*(October), 100197. https://doi.org/10.1016/j.crgsc.2021.100197

Aljeboree, A. M., Alshirifi, A. N., & Alkaim, A. F. (2017). Kinetics and equilibrium study for the adsorption of textile dyes on coconut shell activated carbon. *Arabian Journal of Chemistry, 10*, S3381–S3393. https://doi.org/10.1016/j.arabjc.2014.01.020

Basha, I. K., Abd El-Monaem, E. M., Khalifa, R. E., Omer, A. M., & Eltaweil, A. S. (2022). Sulfonated graphene oxide impregnated cellulose acetate floated beads for adsorption of methylene blue dye: Optimization using response surface methodology. *Scientific Reports, 12*(1). https://doi.org/10.1038/s41598-022-13105-4

Gopal, N., Asaithambi, M., Sivakumar, P., & Sivakumar, V. (2014). Adsorption studies of a direct dye using polyaniline coated activated carbon prepared from Prosopis juliflora. *Journal of Water Process Engineering, 2*, 87–95. https://doi.org/10.1016/j.jwpe.2014.05.008

Guo, D., Li, Y., Cui, B., Hu, M., Luo, S., Ji, B., & Liu, Y. (2020). Natural adsorption of methylene blue by waste fallen leaves of Magnoliaceae and its repeated thermal regeneration for reuse. *Journal of Cleaner Production, 267*, 121903. https://doi.org/10.1016/j.jclepro.2020.121903

Gupta, V. K., Gupta, B., Rastogi, A., Agarwal, S., & Nayak, A. (2011). A comparative investigation on adsorption performances of mesoporous activated carbon prepared from waste rubber tire and activated carbon for a hazardous azo dye-Acid Blue 113. *Journal of Hazardous Materials, 186*(1), 891–901. https://doi.org/10.1016/j.jhazmat.2010.11.091

Ichipi, E. O., Mapossa, A. B., Costa, A. C. F. M., Chirwa, E. M. N., & Tichapondwa, S. M. (2023). Fabrication and characterization of recyclable, magnetic (CoFe2O4)x/Ag2S-ZnO composites for visible-light-induced photocatalytic degradation of methylene blue dye. *Journal of Water Process Engineering, 54*(June). https://doi.org/10.1016/j.jwpe.2023.104040

Iheanacho, O. C., Nwabanne, J. T., Obi, C. C., Igwegbe, C. A., Onu, C. E., & Dahlan, I. (2023). Adsorptive dephenolization of aqueous solutions using thermally modified corn cob: mechanisms, point of zero charge, and isosteric heat studies. *Adsorption Science and Technology, 2023*. https://doi.org/10.1155/2023/2813663

Iqbal, J., Shah, N. S., Sayed, M., Imran, M., Muhammad, N., Howari, F. M., et al. (2019). Synergistic effects of activated carbon and nano-zerovalent copper on the performance of hydroxyapatite-alginate beads for the removal of As 3 þ from aqueous solution. *Journal of Cleaner Production, 235*, 875–886. https://doi.org/10.1016/j.jclepro.2019.06.316

Jain, H., Yadav, V., Rajput, V. D., Minkina, T., Agarwal, S., & Garg, M. C. (2022). An eco-sustainable green approach for biosorption of methylene blue dye from textile industry wastewater by sugarcane bagasse, peanut hull, and orange peel: A comparative study through response surface methodology, isotherms, kinetic, and thermodynamics. *Water, Air, & Soil Pollution, 233*(6), 187. https://doi.org/10.1007/s11270-022-05655-0

Khan, A., Wang, X., Gul, K., Khuda, F., Aly, Z., & Elseman, A. M. (2018). Microwave-assisted spent black tea leaves as cost-effective and powerful green adsorbent for the efficient removal of Eriochrome black T from aqueous solutions. *Egyptian Journal of Basic and Applied Sciences, 5*(2), 171–182. https://doi.org/10.1016/j.ejbas.2018.04.002

Kheddo, A., Rhyman, L., Elzagheid, M. I., Jeetah, P., & Ramasami, P. (2020). Adsorption of synthetic dyed wastewater using activated carbon from rice husk. *SN Applied Sciences, 2*(12), 1–14. https://doi.org/10.1007/s42452-020-03922-5

Kumar, D., Patel, Z., Pandit, P., Pandit, R., Patel, A., Joshi, M., & Joshi, C. (2021). Textile industry wastewaters from Jetpur, Gujarat, India, are dominated by Shewanellaceae, Bacteroidaceae, and Pseudomonadaceae harboring genes encoding catalytic enzymes for textile dye degradation. *Frontiers in Environmental Science, 9*(September), 1–15. https://doi.org/10.3389/fenvs.2021.720707

Mansour, R. A. E. G., Simeda, M. G., & Zaatout, A. A. (2021). Removal of brilliant green dye from synthetic wastewater under batch mode using chemically activated date pit carbon. *RSC Advances, 11*(14), 7851–7861. https://doi.org/10.1039/d0ra08488c

Maruthapandi, M., Kumar, V. B., Luong, J. H. T., & Gedanken, A. (2018). Kinetics, isotherm, and thermodynamic studies of methylene blue adsorption on polyaniline and polypyrrole macro-nanoparticles synthesized by C-dot-initiated polymerization. *ACS Omega, 3*(7), 7196–7203. https://doi.org/10.1021/acsomega.8b00478

Milonjić, S. K., Ruvarac, A. L., & Šušić, M. V. (1975). The heat of immersion of natural magnetite in aqueous solutions. *Thermochimica Acta, 11*(3), 261–266. https://doi.org/10.1016/0040-6031(75)85095-7

Modak, S., Katiyar, P., Yadav, S., & Hans, A. (2023). Valorization of lignocellulosic solid waste obtained from essential oil industry for bio-oil production and dye removal. *Water Practice and Technology, 18*(10), 2384–2400. https://doi.org/10.2166/wpt.2023.154

Momina, M. S., & Suzylawati, I. (2020). Study of the adsorption/desorption of MB dye solution using bentonite adsorbent coating. *Journal of Water Process Engineering, 34*(July 2019). https://doi.org/10.1016/j.jwpe.2020.101155

Montgomery, D. C. (2017). *Design and analysis of experiments*. John wiley & sons.

Oladoye, P. O., Ajiboye, T. O., Omotola, E. O., & Oyewola, O. J. (2022). Methylene blue dye: Toxicity and potential elimination technology from wastewater. *Results in Engineering, 16*(August), 100678. https://doi.org/10.1016/j.rineng.2022.100678

Patidar, K., & Vashishtha, M. (2020). Optimization of process variables to prepare mesoporous activated carbon from mustard straw for dye adsorption using response surface methodology. *Water, Air, & Soil Pollution, 231*(10), 526. https://doi.org/10.1007/s11270-020-04893-4

Sahoo, T. R., & Prelot, B. (2020). Adsorption processes for the removal of contaminants from wastewater: The perspective role of nanomaterials and nanotechnology. In *Nanomaterials for the Detection and Removal of Wastewater Pollutants* (pp. 161–222). Elsevier Inc.. https://doi.org/10.1016/B978-0-12-818489-9.00007-4

Sahu, S., Pahi, S., Tripathy, S., Singh, S. K., Behera, A., Sahu, U. K., & Patel, R. K. (2020). Adsorption of methylene blue on chemically modified lychee seed biochar: Dynamic, equilibrium, and thermodynamic study. *Journal of Molecular Liquids, 315*, 113743. https://doi.org/10.1016/j.molliq.2020.113743

Sharif, K. M., Rahman, M. M., Azmir, J., Mohamed, A., Jahurul, M. H. A., Sahena, F., & Zaidul, I. S. M. (2014). Experimental design of supercritical fluid extraction - A review. *Journal of Food Engineering*. https://doi.org/10.1016/j.jfoodeng.2013.10.003

Subramani, S. E., & Thinakaran, N. (2017). Isotherm, kinetic and thermodynamic studies on the adsorption behaviour of textile dyes onto chitosan. *Process Safety and Environmental Protection, 106*, 1–10. https://doi.org/10.1016/j.psep.2016.11.024

Truzzi, E., Chaouch, M. A., Rossi, G., Tagliazucchi, L., Bertelli, D., & Benvenuti, S. (2022). Characterization and valorization of the agricultural waste obtained from Lavandula steam distillation for its reuse in the food and pharmaceutical fields. *Molecules, 27*(5). https://doi.org/10.3390/molecules27051613

Unugul, T., & Nigiz, F. U. (2020). Preparation and Characterization an Active Carbon Adsorbent from Waste Mandarin Peel and Determination of Adsorption Behavior on Removal of Synthetic Dye Solutions. *Water, Air, and Soil Pollution, 231*(11). https://doi.org/10.1007/s11270-020-04903-5

Xu, R., Mao, J., Peng, N., Luo, X., & Chang, C. (2018). Chitin/clay microspheres with hierarchical architecture for highly efficient removal of organic dyes. *Carbohydrate Polymers, 188*, 143–150. https://doi.org/10.1016/j.carbpol.2018.01.073

Zhu, Y., Yi, B., Yuan, Q., Wu, Y., Wang, M., & Yan, S. (2018). Removal of methylene blue from aqueous solution by cattle manure-derived low temperature biochar. *RSC Advances, 8*(36), 19917–19929. https://doi.org/10.1039/c8ra03018a